INFLUENȚA CONDIȚIILOR DE ÎNTĂRIRE A BETONULUI CELULAR AUTOCLAVIZAT ASUPRA FORMĂRII TOBERMORITULUI
INFLUENCE OF HARDENING CONDITIONS OF AUTOCLAVED AERATED CONCRETE ON TOBERMORITE FORMATION

M. BALTAKYS* , R. SIAUCIUNAS, A. EISINAS
Department of Silicate Technology, Faculty of Chemical Technology, Kaunas University of Technology, Radvilenu str. 19, LT-50254, Kaunas, Lithuania

The influence of hardening conditions on the mineralogical composition and mechanical properties of AAC were examined. Samples with dimensions 100x100x100 mm from industrial cakes were cut and hardened at saturated steam pressure for 4–16 h at 170–200 °C temperatures. The biggest quantity of 1.13 nm tobermorite and C-S-H (I) was formed after 8 h of treatment at 180 °C temperature and AAC samples reached the highest compressive strength. The morphology of tobermorite depends on temperature: at 200 °C the surface of pores is covered with fibrous shape crystals and the mixture of plate shape crystals together with fibrous crystals and amorphous aggregates is formed in the structure material, while at 180 °C platy shape crystals are formed in all samples. It was estimated too, that thermal shrinkage of samples, hardened at 200 °C, decreased twice. The products were characterized by XRD, STA, SEM, MIP and dilatometric analysis

***Keywords**: Aerated concrete, Compressive strength, Structural analysis, Tobermorite*

1. Introduction

In recent years, the increasing requirement for flexibility, comfort and energy saving in residential and industrial buildings has led both designers and manufacturers to adopt new constructive systems, for instance, autoclaved aerated concrete (AAC) masonry. AAC is obtained by using inorganic binders such as cement and/or lime combined with fine siliceous based material, cell-generating material and water [1]. Prepared mixture cured under saturated water steam in autoclaves at 170-200 °C temperature [2]. The aluminum paste reacts with calcium hydroxide to form hydrogen gas in the making of aerated concrete, as follows [3, 4]:

$$2Al+3Ca(OH)_2+6H_2O \rightarrow 3CaO \cdot Al_2O_3 \cdot 6H_2O+3H_2 \quad \text{(Eq. 1)}$$

With extremely low density (300-500 kg/m^3) and thermal conductivity (0.100 W/(m·K)), aerated concrete is an ideal material for thermal insulation and sound-proofing [5-7]. Aerated concrete can be used for floors, trench fills, roof insulation [8, 9] and other insulating purposes, as well as for making masonry units [10]. Among the factors affecting the compressive strength of AAC, there are shapes and sizes, the gas generation method, the installation direction, the water content and the curing process. In addition, the structure of the air pores and the mechanical condition of the pore shells directly affect the compressive strength [11].

During the hydrothermal treatment for several hours [12], the formation of tobermorite occurs, the chemical formula of which is $5CaO \cdot 6SiO_2 \cdot 5H_2O$ [13]. This calcium silicate hydrate strongly influences mechanical properties of the final product. During the initial autoclaving stage, the silica-based compounds such as amorphous silica, improve the polymerization of semi-crystalline calcium silicate hydrate (C-S-H) compounds, preceding the direct formation of tobermorite. On the other hand, the presence of aluminum delays the initial formation of the CSH-based compounds reducing the solubility of quartz, yet accelerating a direct formation of tobermorite [14].

The synthesis of tobermorite under hydrothermal conditions has been extensively studied for various starting materials including several types of silica sources and various additives [15]. It has been revealed that Al compounds have significant effects on the tobermorite formation process [14]. J. H. Houston et. al. [16] determined that the formation of tobermorite proceeds through three stages: formation of amorphous and non-crystalline CSH, growth of semi-crystals of tobermorite and recrystallization of tobermorite in a solid phase. As K. Matsui et. al. [17] suggested, different reaction paths for the formation of tobermorite in an AAC system exist. In one of them, tobermorite appears when the temperature reaches 190 °C, in other

* Autor corespondent/*Corresponding author*,
E-mail: marius.baltakys@ktu.edu

words, when amorphous gel-based CSH begin to decrease. The amount of tobermorite is maximum at the end of the autoclave process.

Furthermore, the formation of calcium silicate hydrates is more difficult in the industrial AAC production because of various impurities in raw materials [17]. Thus, the formation mechanism of these compounds is not completely understood. If a great amount of tobermorite forms in AAC samples during hardening process, the operating temperature of samples increases, in comparison with products in which C-S-H(I) are dominated. In this work, the influence of different hardening conditions on the mechanical and mineralogical properties of AAC samples was examined.

2.Materials and Methods

2.1. Materials

The raw materials used for preparation of forming mixtures of autoclaved aerated concrete were: Portland cement CEM I 42.5 N (SC "Akmenes cementas", Lithuania) of the following mineralogical composition (in wt. %): $3CaO{\cdot}SiO_2$=57.27; $2CaO{\cdot}SiO_2$=16.28; $3CaO{\cdot}Al_2O_3$=8.81; $4CaO{\cdot}Al_2O_3{\cdot}Fe_2O_3$=9.94 according to the standard [18]; milled lime CL90-Q (JSC "Lhoist Bukowa", Poland) with CaO in 91.03 %, reactivity expressed by time 9.07 min. and temperature 60.2 °C according to the standard [19]; gypsum (JSC "Dolina Nidy", Poland) with 89.97 % of $CaSO_4{\cdot}2H_2O$ according to the standard [20]; milled quartz sand (JSC "Matuizu plytine", Lithuania) with 84. 08 % of SiO_2 and fineness of 2200 cm^2/g according to the standard [21]. Such fineness was obtained by milling in ball mill (capacity of 38.64 m^3, metal balls of 35.0 mm diameter). In forming mixtures, as gas-generating agent, aluminum pastes (JSC "Benda-Lutz", Poland) 5-6380/80 (average particle size –24.0 μm) and 5-6355/80 (average particle size –48.0 μm) with 70 % of pure aluminum were used. Before addition to the forming mixture, aluminum pastes were mixed with ratio 1:1 and dispersed for 30 minutes in water (aluminum/water ratio 1:20) using tank of 0.75 m^3 capacity.

2.2. Preparation of forming mixtures and concrete samples

The forming mixture was prepared and mixed in the industrial production line and its composition was selected on the basis of the industrial recipe, %: Portland cement – 16.2, lime – 12.8, gypsum – 2.3, sand slurry – 50.0, return slurry – 18.7. The water/solids ratio was equal to 0.675; content of aluminum paste was amounted to 0.11 % by weight of solids dry mass.

All required amount of raw materials was weighed at the beginning of mixing. The components of forming mixture were mixed in the high speed vertical propeller stirrer of 5 m^3 volume by the speed of 1500 rpm. First, required quantities of sand and return slurries were mixed with cold and hot water together (to achieve the temperature mean of 40 °C). Second, Portland cement, lime and gypsum were added. Finally, aluminum paste suspension was placed. Overall mixing time was 3.05 minutes. After mixing, homogenized forming mixture was poured into the steel moulds (size 6220x1580x700 mm). The poured moulds were transported to the fermentation area (38 °C temperature) and kept in moulds for 160 min. Later, the heap of forming mixture was cut off. The samples were cut into 100 x 100 x 100 mm cubes and hardened in the laboratory autoclave of 20 l capacity in the specified mode (2.5 + (4-6-8-12-16) + 2.5), at water vapour temperature of 170, 180 and 200 °C.

After hardening, the samples were dried to the constant mass in the conditioning oven at the temperature of 105 ± 5 °C.

2.3. Methods of testing

The compressive strength of AAC samples was determined according to the requirements of the standard [22]. The press MEGA 10-400-50 (FORM+TEST GmbH) was used. The loading rate of samples during compression was 50 N/s until the destruction of the sample. 3 samples of each batch were subjected to testing. The volume density of the samples was determined according to the requirements of the standard [23].

For the mineralogical analysis, dry samples were sieved through a sieve with an 80 μm mesh. The XRD analysis was performed using the D8 Advance diffractometer (Bruker AXS, Karlsruhe, Germany) operating at the tube voltage of 40 kV and tube current of 40 mA. The X-ray beam was filtered with a Ni 0.02 mm filter to select the CuKα wavelength. Diffraction patterns were recorded in a Bragg-Brentano geometry using a fast counting detector Bruker LynxEye based on the silicon strip technology. The specimens of samples were scanned over the range 2θ = 3–70° at a scanning speed of 6° min^{-1} using a coupled two theta/theta scan type.

Simultaneous thermal analysis (STA) (differential scanning calorimetry and thermogravimetry) was carried out on a Linseis STA PTI1000 instrument with ceramic sample handlers and crucibles of Pt at a heating rate of 15 °C/min, the temperature ranging from 30 °C to 900 °C under the ambient atmosphere.

The sample microstructure was investigated by using the field-emission scanning electron microscope SEM JSM-7600F (JOEL). The split surface of the samples was tested, using low accelerating voltage (10 kV).

The porosity and pore size distribution of the samples were measured by mercury intrusion porosimetry (MIP, Micromeritics, AutoPore 9500

IV). The pressure greater than 400 MPa can be achieved by the calorimetry apparatus and allows the mercury to penetrate pores as fine as 0.003l m in diameter [24].

The dilatometric (DIL) analysis was performed by using the Linseis "L75H1600 Platinum series" with Al_2O_3 sample holder and pushrod. Cylindrical dilatometric samples of 5 mm diameter and 22 mm length were heated to 1000 °C at a heating rate of 10 °C/min to monitor the sample change under air atmosphere.

3. Results and Discussion

3.1. Mechanical and mineralogical analysis

The average values of compressive strength of AAC samples are shown in Figure 1. It was found that after 8 hours of the hydrothermal treatment at 170 °C temperature, the compressive strength of sample was equal to 2.58 MPa (Fig. 1). After increasing the hydrothermal treatment temperature to 180 °C, the compressive strength increased and reached the maximum value after 8 h of curing (3.97 MPa). Later on, by prolonging the duration of treatment to 16 h the compressive strength slightly decreased to 3.74 MPa. Meanwhile, the further increment of the reaction temperature to 200 °C led to even lower values of mentioned parameter (~ 30 %). The further decrease in the compressive strength was also observed by prolonging the isothermal curing from 8 to 16 h. On the other hand, the density of AAC samples was very similar and varied in the 470–481 kg/m^3 range.

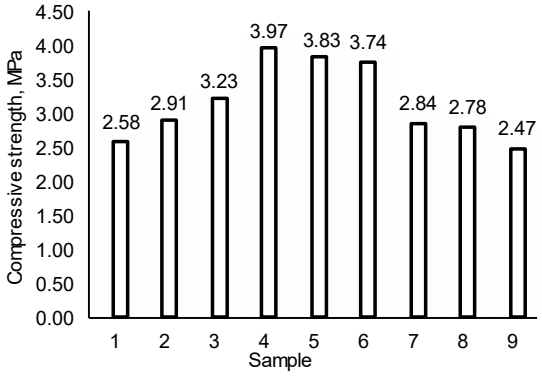

Fig.1 - The influence of hardening conditions on the compressive strength of AAC samples, when the isothermal temperature and duration of hardening were: 1 – 170 °C, 8 h; 2 – 180 °C, 4 h; 3 – 180 °C, 6 h; 4 – 180 °C, 8 h; 5 – 180 °C, 12 h; 6 – 180 °C, 16 h; 7 – 200 °C, 8 h; 8 – 200 °C, 12 h; 9 – 200 °C, 16 h.

It is known that the compressive strength of AAC mainly depends on the quantity and quality of tobermorite group minerals (semi crystalline C-S-H (I) and 1.13 nm tobermorite), which forms during the hydrothermal treatment [13]. Thus, in order to estimate the mineralogical composition of AAC samples, XRD, STA and SEM analysis were performed.

It was determined that a moderate amount of 1.13 nm tobermorite forms already after 8 h of the hydrothermal treatment at 170 °C temperature in the AAC sample (*d*-spacing – 1.133; 0.506; 0.297; 0.253; 0,241; 0.209; 0,198; 0.185; 0.167) (Fig. 2, curve 1). A similar amount of mentioned compound also remains after 4 and 6 hours of the autoclaving treatment at 180 °C temperature (Fig. 2, curves 2 and 3). However, after extending the duration of the treatment to 8 h the amount of formed 1.13 nm tobermorite noticeably increased (Fig. 2, curve 4). In addition, a large amount of other compound, namely, semi crystalline calcium silicate hydrate C-S-H (I) with high binding properties remained in the sample (Fig. 3, a and b.; curve 1).

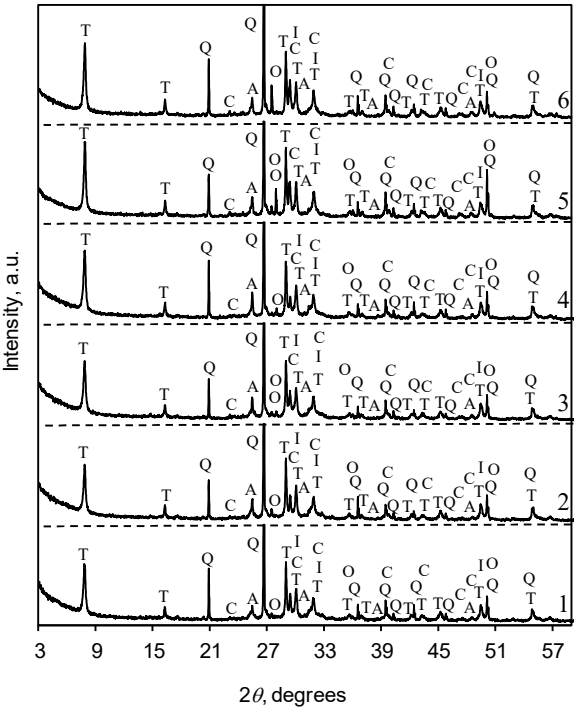

Fig.2 - X-ray diffraction patterns of AAC samples, when the isothermal temperature and duration of hardening were: 1 – 170 °C, 8 h; 2 – 180 °C, 4 h; 3 – 180 °C, 6 h; 4 – 180 °C, 8 h; 5 – 180 °C, 12 h; 6 – 180 °C, 16 h. Indexes: T – 1.13 nm tobermorite; Q – quartz; A – anhydrate; C – calcite; O – orthoclase; I – C-S-H (I).

The quantity of 1.13 nm tobermorite narrowly but coherently decreased after extending the duration of the hydrothermal treatment to 12 and 16 h: the area and intensity of the main 1.13 nm tobermorite diffraction peak (*d*-spacing – 1.133) slightly decreased: from 12.700 to 11.510 a. u. and from 41.2 to 38.5 a. u., respectively, as well as the heat of exothermic effect assigned to C-S-H (I) recrystallization to wollastonite (847 – 834 °C) decreased from 82 to 23 J/g (Fig. 3, curves 1 and 3).

In addition, under all hydrothermal treatment conditions, these compounds were also identified: anhydrite (*d*-spacing – 0.350; 0.284; 0.233; 0.187); $CaCO_3$ (*d*-spacing – 0.385; 0.303; 0.228; 0.209; 1.191 0.187); orthoclase (*d*-spacing – 0.324;

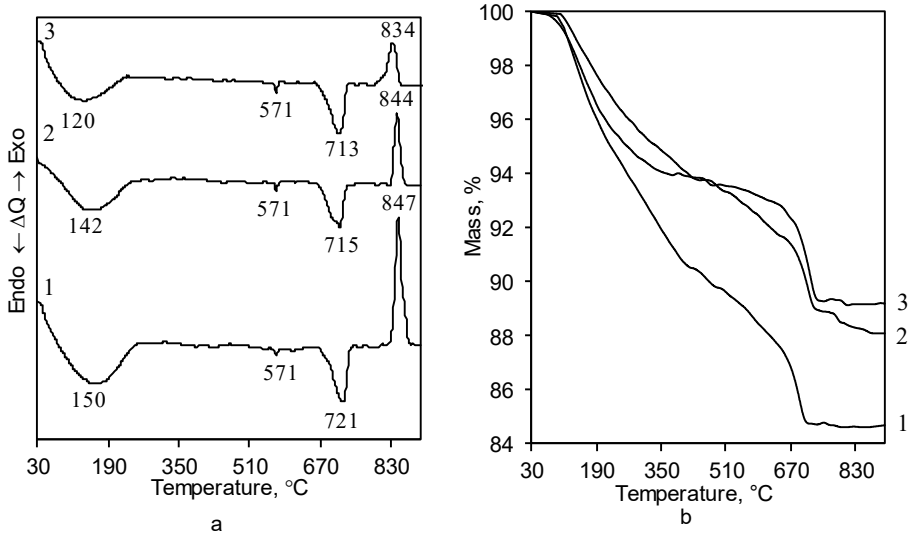

Fig.3 - DSC (a) and TG (b) curves of AAC samples, when duration of the hydrothermal treatment at 180 °C is: 1 – 8 h; 2 – 12 h; 3 – 16 h.

0.319; 0.252; 0.182) and quartz (*d*-spacing – 0.426; 0.334; 0.246; 0.228; 0.224; 0.213; 0.198; 0.182; 0.167) (Fig. 2).

The above mentioned results were confirmed by STA analysis data (Fig. 3). On DSC curves at 100 – 250 °C temperature range, the broad endothermic peak is related to the loss of physisorbed and interlayer water from the crystal structure of C-S-H (I) and 1.13 nm tobermorite. This data is also in good agreement with the study performed by S. Shaw et al., on a natural sample of tobermorite. These authors observed an endothermic hump in DSC curve associated with a weight loss of about 9 wt. % up to 250 °C temperature. During this process, the mass loss in TG curve is the greatest (6.70 %), when the duration of samples synthesis is 8 h (Fig. 3, b, curve 1). The second endothermic effect was observed at 571 °C, which is attributed to α-β modifications transition of quartz. An exothermic effect at ~843 °C temperature, which is assigned to the recrystallization of C-S-H (I) to wollastonite varied in a narrow range. Moreover, at ~712 °C due to the decarbonation of hardening products, a fair amount of calcium carbonate was also observed.

Significant changes in the mineralogical composition were observed, when the temperature of the isothermal curing was increased to 200 °C (Fig. 4). After 8 h of the isothermal curing, the intensities of the main diffraction peak characteristic to 1.13 nm tobermorite, in comparison with 180 °C temperature, were decreased.

Moreover, after increasing the duration of treatment, the amount of mentioned compound negligible but coherently decreases (Fig. 4, curves 2 and 3). Furthermore, the transfer of calcium sulfate dehydrate to anhydrite is finished in this temperature because peak intensities of this compound increased almost 2.5 times (Fig. 2 and 4). Anhydrite did not have binding properties.

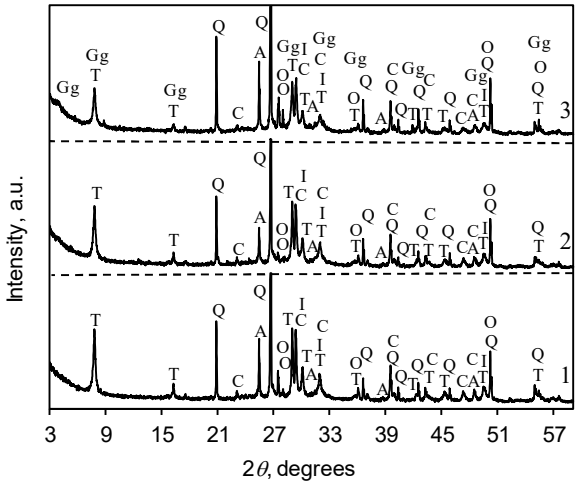

Fig.4 - X-ray diffraction patterns of AAC samples, when duration of the hydrothermal treatment at 200 °C is: 1 – 8 h; 2 – 12 h; 3 – 16 h. Indexes: T – 1.13 nm tobermorite; Q – quartz; A – anhydrite; C – calcite; O – orthoclase; I – C-S-H (I).

Furthermore, the visible changes can be seen after 16 hours of hardening because traces of a new compound of calcium silicate hydrate gyrolite gel (*d*-spacing – 2.225; 1.130; 0.545; 0.308; 0.280; 0.249; 0.213; 0.184; 0.167) (Fig. 4, curve 3) were formed. This compound also does not have binding properties. At the same time, the area (4.739 a. u.) and intensity (14.8 a. u.) in the X-Ray patterns, as well as crystallite size (156.6 nm) of 1.13 nm tobermorite, significantly decreased. The main explanation for this is that, by increasing the temperature and duration of the hydrothermal treatment, greater amount of quartz reacts and the C/S molar ratio of products decreased and low basicity compounds are formed. Besides, in these hydrothermal treatment conditions decreased quantity of other compound with binding properties C-S-H (I) (Fig. 5, a): increasing the temperature of the hydrothermal treatment from 180 to 200 °C, the mass loss in the

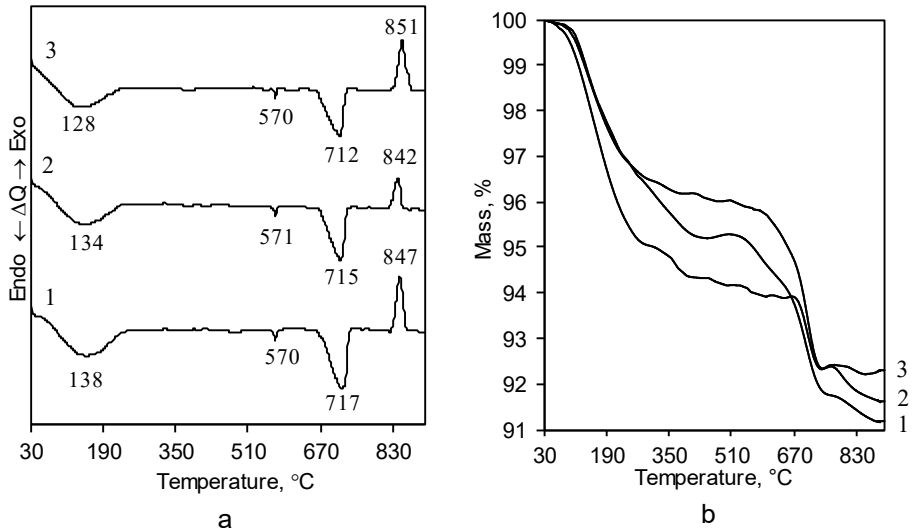

Fig. 5 - DSC (a) and TG (b) curves of AAC samples, when duration of the hydrothermal treatment at 200 °C is: 1 – 8 h; 2 – 12 h; 3 – 16 h.

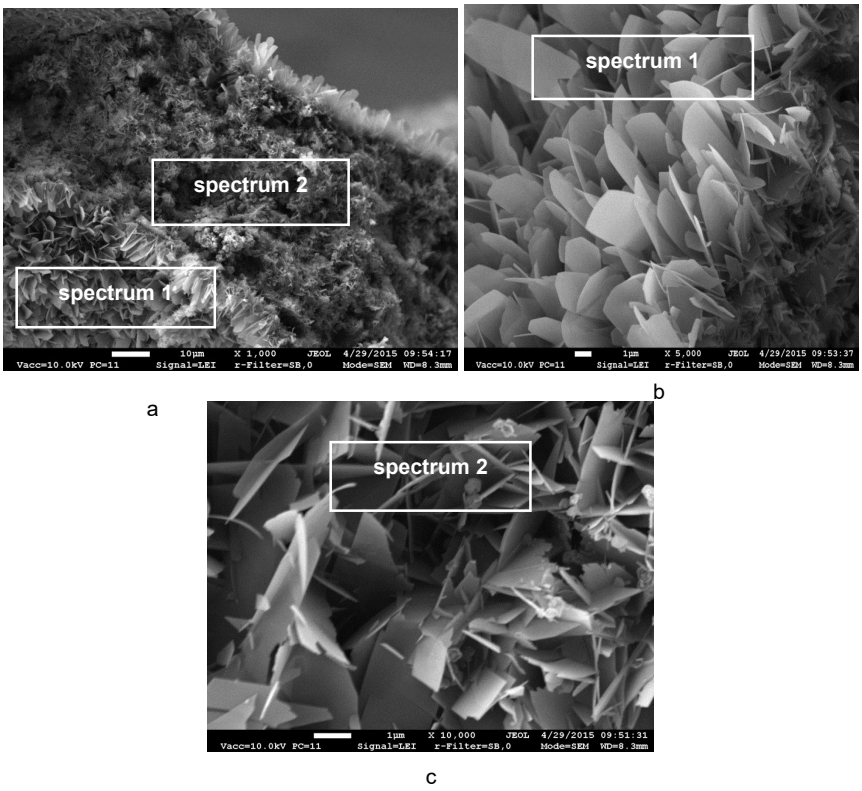

Fig. 6 - SEM micrographs of AAC sample cured 8 h at 180 °C temperature (a), spectrum 1 (b) and spectrum 2 (c).

100 – 250 °C temperature range decreased from 6.70 to 3.15 % (Figure 3, b, curve 1; Figure 5, b, curve 1) and the heat of the exothermic effect changed almost twice.

Thus, XRD and STA data showed that in AAC samples hardened at 200 °C temperature formed the compounds having more inert (anhydrite and gyrolite) and less binding properties (1.13 nm tobermorite and C-S-H (I)), in comparison with the samples treated at 180 °C.

In order to estimate the morphology of formed compounds, SEM analysis was performed (Fig. 6 and 7). It was found that after 8 h of curing at 180 °C the surface of pores in the AAC samples is covered with plate shape crystals (Fig. 7, a and b), as well as structure material (between pores) (Fig. 7, c). Similar results were obtained by other authors: platy deposits are a crystal habit of tobermorite with a size of approximately 5μm [25, 26]. This is in a good agreement with XRD analysis data, as under the conditions mentioned above, the intensity of the main diffraction peak of 1.13 nm tobermorite was the highest one.

Meanwhile, by increasing the temperature and duration of treatment (200 °C, 16 h), the form of crystals was changed (Fig. 7, c). Platelike shape

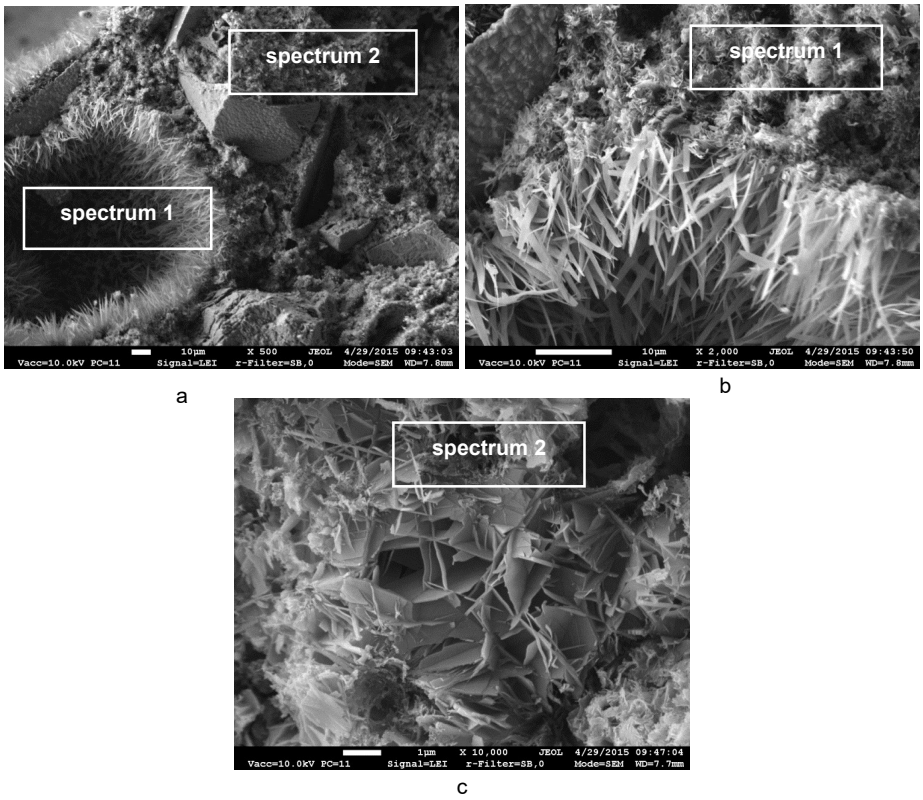

Fig. 7 - SEM micrographs of AAC samples cured 16 h at 200 °C temperature (a), spectrum 1 (b) and spectrum 2 (c).

crystals together with fibrous crystals and amorphous aggregates were identified in structure material (Fig. 7, c). The latest, presumably are associated with gyrolite gels. These results coincide with XRD analysis and compressive strength data (Fig 1 and 4). The surface of pores is covered only with fibrous shape crystals (Fig. 7, a and b). This data also corresponds other author's results: the tobermorite phase can have either a platelet or fibrous morphology [27].

N. S. Bell et. al. [28] have noticed in their work that morphological differences of tobermorite could lie in the mechanism of nucleation. Platelets may result from heterogeneous nucleation and fibres from homogeneous nucleation. A second possibility exists in which the two morphologies result from differences in the number of cross-linking Si-O-Si bonds.

As can be noted, the decrement of mechanical product strength can influence not only the changes of mineralogical composition but the texture as well (pore diameter, form etc.).

In order to determine the volume of micropores and their diameter in AAC samples, the mercury intrusion porosimetry analysis was performed. It was estimated that micropores with diameter 0.6-0.0065 μm are dominated in all samples and these pores compose 49 – 52 % of all micropores in the samples autoclaved at 180 °C temperature. It should be noted that the pores of the mentioned diameter increased up to 8 % (54 – 58 %) after the increment of the curing temperature

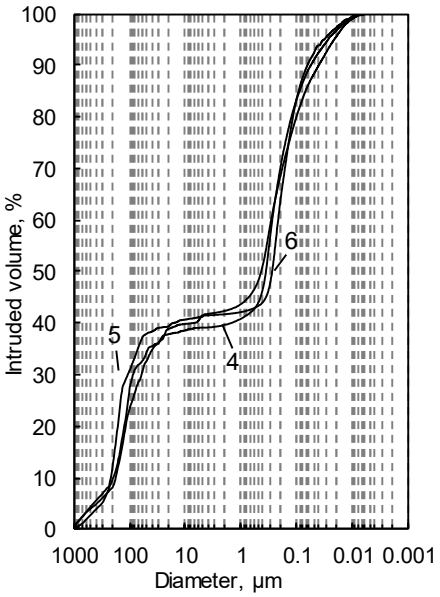

Fig.8 - Dependence of volume of micropores in AAC samples on their diameter, when the isothermal temperature and duration of hardening were: 4 – 200 °C, 8 h; 5 – 200 °C, 12 h; 6 – 200 °C, 16 h.

to 200 °C (Fig. 8).

The temperature of the hydrothermal treatment (180 or 200 °C) does not have any significant influence on the micropores with the diameter of 0.6 – 40 μm (8 – 10 %) and 40 – 1000 μm (35 – 45 %).

Finally, thermal shrinkage of AAC samples was investigated (Fig. 9). All samples are shrinking similar to 800 °C temperature (1.05 – 1.36 %) but

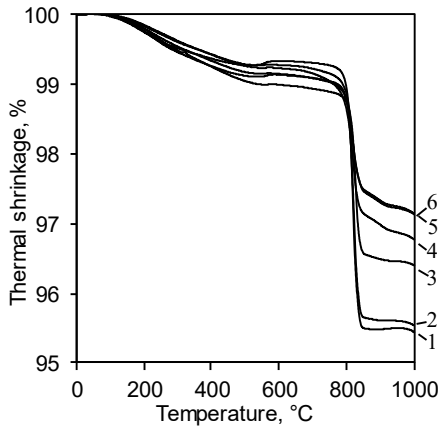

Fig.9 - Thermal shrinkage of AAC, when the isothermal temperature and duration of hardening were: 1 – 180 °C, 8 h; 2 – 180 °C, 12 h; 3– 180 °C, 16 h; 4 – 200 °C, 8 h; 5 – 200 °C, 12 h; 2 – 200 °C, 16 h.

after increment of burning temperature significant differences were determined. For instance, shrinkage (in the range of 800 – 1000 °C burning temperature) of samples treated at 200 °C temperature for 16 h is 1.70 %, whereas samples autoclaved at 180 °C for 8 h – 3.51 % (Fig. 9, curves 1 and 6).

Therefore, thermal shrinkage of samples hardened at lower temperature increased twice. This could be explained as follows: lower amount of C-S-H (I) is formed in the AAC samples cured at higher temperature and later compound intensively shrinks with recrystallization to wollastonite at higher than 800 °C temperature. Thus, AAC samples with lower thermal shrinkage could be used for structures, requiring greater resistance of the products.

4. Conclusions

1. It was found that after 8 h of the hydrothermal treatment at 180 °C temperature 1.13 nm tobermorite and C-S-H(I) are the main products in autoclaved aerated concrete samples and they have the highest compressive strength. Meanwhile, after changing the temperature and duration of the isothermal curing, the formation of these compounds and values of compressive strength decreased.
2. It was determined that platy shape crystals characteristic to 1.13 nm tobermorite are formed after synthesis at 180 °C temperature. Meanwhile, the morphology of crystals changed by increasing temperature to 200 °C: the surface of pores is covered only with fibrous shape crystals and mixture of plate like shape crystals together with fibrous crystals and amorphous aggregates is formed in the structure material.
3. It was estimated that significantly lower amount of semi-crystalline C-S-H (I) remained in the AAC samples after increasing the temperature of the hydrothermal treatment from 180 to 200 °C, therefore, thermal shrinkage of samples decreased twice. In addition, it is recommended to harden AAC products at 200 °C temperature for the application in the areas, where the operating temperature reaches 600 – 650 °C.

REFERENCES

1. European standard LST EN 771-4:2011. Specification for masonry units-Part 4: Autoclaved aerated concrete masonry units, 2011.
2. A. Penna, M. Mandirola, M. Rota, G. Magenes, Experimental assessment of the in-plane lateral capacity of autoclaved aerated concrete (AAC) masonry walls with flat-truss bed-joint reinforcement, Construction and Building Materials, 2015, **82**, 155.
3. W. Wongkeo, P. Thongsanitgarn, K. Pimraksa, A. Chaipanich, Compressive strength, flexural strength and thermal conductivity of autoclaved concrete block made using bottom ash as cement replacement materials, Materials and Design, 2012, **35**,434..
4. N. Narayanan, K. Ramamurthy, Structure and properties of aerated concrete: a review, Cement and Concrete Composites, 2000, **22**, 321.
5. T. Mitsuda, K. Sasaki, H. Ishida, Phase evolution during autoclaving process of aerated concrete, Journal of American Ceramic Society, 1992, **75**(7),1858.
6. L. Ropelewski, R. Neufeld, Thermal inertia properties of autoclaved aerated concrete, Journal of Energy Engineering, 1999, **125:2**(59), 59.
7. M. A. Mousa, N. Uddin, Experimental and analytical study of carbon fiberreinforced polymer (FRP)/autoclaved aerated concrete (AAC) sandwich panels, Engineering Structures, 2009, **31**, 2337.
8. Y. Song, C. Guo, J. Qian, T. Ding, Effect of the Ca-to-Si ratio on the properties of autoclaved aerated concrete containing coal fly ash from circulating fluidized bed combustion boiler, Construction and Building Materials, 2015, **83**, 136.
9. Y. Feng, Thermal design standards for energy efficiency of residential buildings in hot summer/cold winter zones, Energy and Buildings, 2004, **36**, 1309.
10. J. A. Hess, L. Kincl, T. Amasay, P. Wolfe, Ergonomic evaluation of masons laying concrete masonry units and autoclaved aerated concrete, Applied Ergonomics, 2010, **41**(3), 477.
11. Z. O. Pehlivanli, I. Uzun, I. Demir, Mechanical and microstructural features of autoclaved aerated concrete reinforced with autoclaved polypropylene, carbon, basalt and glass fiber, Construction and Building Materials, 2015, **96**, 428.
12. F. Bisceglie, E. Gigante, M. Bergonzoni, Utilization of waste Autoclaved Aerated Concrete as lighting material in the structure of a green roof, Construction and Building Materials, 2014, **69**, 351.
13. F. Matsushita, Y. Aono, S. Shibata, Carbonation degree of autoclaved aerated concrete, Cement and Concrete Research, 2000, **30**, 1741..
14. M. W. Grutzeck, M. Scheffler, P. Colombo, Structure, manufacturing, properties and applications, Cellular ceramics, 2006, doi: 10.1002/3527606696.ch2i.
15. S. Shaw, S. M. Clark, C. M. B. Henderson, Hydrothermal formation of the calcium silicate hydrates, tobermorite ($Ca_5Si_6O_{16}(OH)_2 \cdot 4H_2O$) and xonotlite ($Ca_6Si_6O_{17}(OH)_2$): An insitu synchrotron study, Chemical Geology, 2000, **167**(1), 129.
16. J. R. Houston, R. S. Maxwell, S. A. Carroll, Transformation of meta-stable calcium silicate hydrates to tobermorite: reaction kinetics and molecular structure from XRD and NMR spectroscopy, Geochemical Transactions, 2009, **10**, 1.
17. K. Matsui, A. Ogawa, J. Kikuma, M. Tsunashima, T. Ishikawa, S. Matsuno, Insitu time-resolved X-ray diffraction of tobermorite formation in autoclaved aerated concrete: influence of silica source reactivity and Al addition, Cement and Concrete Research, 2011, **41**, 510.
18. European standard LST EN 197-1:2011. Cement - Part 1: Composition, specifications and conformity criteria for common cements, 2011.
19. European standard LST EN 459-2:2010. Building lime - Part 2: Test methods, 2010.
20. European standard LST EN 13279-1:2008. Gypsum binders and gypsum plasters - Part 1: Definitions and requirements, 2008.
21. Lithuanian standard LST 1273:2009. Sand for calcium silicate and autoclaved aerated concrete products. Specifications and test methods, 2009.
22. European standard LST EN 772-1:2011+A1:2015. Methods of test for masonry units - Part 1: Determination of compressive strength, 2011 and 2015.
23. European standard LST EN 772-13:2003. Methods of test for masonry units - Part 13: Determination of net and gross dry density of masonry units (except for natural stone), 2003.
24. P. Wenshi, L. Gaokui, Atlas of mineral infrared spectroscopy, Science press, Beijing, 1982.
25. S. Shaw, C. M. B. Henderson, B. U. Komanschek, Dehydration/recrystallization mechanisms, energetics, and kinetics of hydrated calcium silicate minerals: an in situ TGA/DSC and synchrotron radiation SAXS/WAXS study, Chemical Geology, 2000, **167**, 141.
26. N.Y. Mostafa, A.A. Shaltout, H. Omar, S.A. Abo-El-Enein, Hydrothermal synthesis and characterization of aluminium and sulfate substituted 1.1 nm tobermorites, Journal of Alloys and Compounds, 2009, **467**(1-2), 332.
27. H. Maeda, K. Abe, E. H. Ishida, Hydrothermal synthesis of aluminum substituted tobermorite by using various crystal phases of alumina, Journal of the Ceramic Society of Japan, 2011, **119**(5), 375.
28. N. S. Bell, S. G. Venigalla, M. P. Gill, J. H. Adair, Morphological forms of tobermorite in hydrothermally treated calcium silicate hydrate gel, Journal of American Ceramic Society, 1996, **79**(8), 2175.